Combustion and Flame 160 (2013) 970–981

Contents lists available at SciVerse ScienceDirect

Combustion and Flame

journal homepage: www.elsevier.com/locate/combustflame

Experimental and quantum mechanics investigations of early reactions of monomethylhydrazine with mixtures of NO_2 and N_2O_4

Wei-Guang Liu [a], Shiqing Wang [b], Siddharth Dasgupta [a], Stefan T. Thynell [b,*], William A. Goddard III [a,*], Sergey Zybin [a], Richard A. Yetter [b]

[a] Materials and Process Simulation Center (MSC), Beckman Institute (139-74), California Institute of Technology, Pasadena, CA 91125, United States
[b] Department of Mechanical and Nuclear Engineering, The Pennsylvania State University, University Park, PA 16802, United States

ARTICLE INFO

Article history:
Received 25 September 2012
Received in revised form 6 January 2013
Accepted 18 January 2013
Available online 15 February 2013

Keywords:
Hypergolic propellant
Monomethylhydrazine
Nitrogen dioxide
Pre-ignition reactions
Quantum mechanics

ABSTRACT

The gas-phase chemistry of the hypergolic system CH_3NHNH_2 – monomethylhydrazine (MMH), with oxidizers NO_2/N_2O_4 at room temperature and 1 atm N_2 was investigated experimentally using a gold-coated chamber reactor, coupled with a Fourier transform infrared (FTIR) spectrometer. The IR-active species identified in the early reactions include HONO, monomethylhydrazinium nitrite (MMH·HONO), methyl diazene ($CH_3N{=}NH$), methyl nitrate (CH_3ONO_2), methyl nitrite (CH_3ONO), nitromethane (CH_3NO_2), methyl azide (CH_3N_3), H_2O, N_2O and NO. In order to elucidate the mechanisms by which these observed products are formed, we carried out quantum mechanics calculations [CCSD(T)/M06-2X] for the possible reaction pathways. Based on these studies, we propose that the oxidation of MMH in an atmosphere of NO_2 occurs via two mechanisms: (1) sequential H-abstraction and HONO formation, and (2) reaction of MMH with asymmetric $ONONO_2$, leading to formation of methyl nitrate. These mechanisms successfully explain all intermediates observed experimentally. We conclude that the formation of asymmetric $ONONO_2$ is assisted by an aerosol formed by HONO and MMH that provides a large surface area for $ONONO_2$ to condense, leading to the generation of methyl nitrate. Thus we propose that the overall pre-ignition process involves both gas-phase and aerosol-phase reactions.

1. Introduction

Hypergolic bipropellants are fuel-oxidizer combinations that ignite spontaneously upon mixing at ambient temperatures. They facilitate the design of rocket thrusters by simplifying the ignition system, and are widely used in propulsion systems in which variable and/or intermittent thrust capabilities are needed. Among the most commonly deployed bipropellant combinations is monomethylhydrazine/nitrogen tetroxide, which is also referred to as MMH/NTO or CH_3NHNH_2/N_2O_4 [1] For applications in which the freezing point of NTO is too high, an alternative oxidizer is red fuming nitric acid (RFNA), which is composed of nitric acid (HNO_3, ~85 wt%) and NO_2 (8–15 wt%).

Recently the impinging stream vortex engine (ISVE) has attracted significant attention due to its compact size and potential for efficient combustion, making it important to develop computational fluid dynamics (CFD) models to gain insight into the influence of design parameters on engine performance [2–5]. An important part of this effort is to develop a chemical kinetics mechanism for MMH/NTO or MMH/RFNA combinations.

To provide a starting point for such activities a detailed, finite-rate, chemical kinetics mechanism of MMH/RFNA was developed by the U.S. Army Research Laboratory (ARL) [6–9] for modeling the gas-phase combustion processes. The most recent version of this mechanism involves 513 reactions and 81 species [6]. Sources for the ARL mechanism include the following:

1. a set of reactions for H/C/N/O compounds developed by Anderson and co-workers for modeling the dark zones observed in solid-propellant combustion (43 species, 204 reactions) [10],
2. approximately 160 small-hydrocarbon-molecule reactions that were extracted from the GRI 3.0 database [11],
3. approximately 80 reactions involving HNO_3, NO_3, N_2O_4, and hydrocarbon/NO_x moieties that were identified via a literature search performed specifically for the mechanism development effort, and
4. approximately 50 reactions recommended by Catoire and co-workers for modeling the ignition and combustion of MMH/O_2 [12] and MMH/NTO [13] systems.

The validity and completeness of the ARL mechanism was tested by running CHEMKIN [14] simulations for MMH/NTO systems, and a reduced version of the mechanism was used in CFD simulations for the ISVE engine [2,5,8].

* Corresponding authors.
E-mail addresses: Thynell@psu.edu (S.T. Thynell), wag@wag.caltech.edu (W.A. Goddard III).

0010-2180/$ - see front matter © 2013 The Combustion Institute. Published by Elsevier Inc. All rights reserved.
http://dx.doi.org/10.1016/j.combustflame.2013.01.012

Report Documentation Page

Form Approved
OMB No. 0704-0188

1. REPORT DATE	2. REPORT TYPE	3. DATES COVERED
FEB 2013		**00-00-2013 to 00-00-2013**

4. TITLE AND SUBTITLE	5a. CONTRACT NUMBER
Experimental and quantum mechanics investigations of early reactions of monomethylhydrazine with mixtures of NO2 and N2O4	5b. GRANT NUMBER
	5c. PROGRAM ELEMENT NUMBER
6. AUTHOR(S)	5d. PROJECT NUMBER
	5e. TASK NUMBER
	5f. WORK UNIT NUMBER
7. PERFORMING ORGANIZATION NAME(S) AND ADDRESS(ES) **California Institute of Technology,Materials and Process Simulation Center (MSC),Pasadena,CA,91125**	8. PERFORMING ORGANIZATION REPORT NUMBER
9. SPONSORING/MONITORING AGENCY NAME(S) AND ADDRESS(ES)	10. SPONSOR/MONITOR'S ACRONYM(S)
	11. SPONSOR/MONITOR'S REPORT NUMBER(S)

12. DISTRIBUTION/AVAILABILITY STATEMENT
Approved for public release; distribution unlimited

13. SUPPLEMENTARY NOTES

14. ABSTRACT

The gas-phase chemistry of the hypergolic system CH3NHNH2 ? monomethylhydrazine (MMH), with oxidizers NO2/N2O4 at room temperature and 1 atm N2 was investigated experimentally using a gold-coated chamber reactor, coupled with a Fourier transform infrared (FTIR) spectrometer. The IR-active species identified in the early reactions include HONO, monomethylhydrazinium nitrite (MMH HONO), methyl diazene (CH3N@NH), methyl nitrate (CH3ONO2), methyl nitrite (CH3ONO), nitromethane (CH3NO2) methyl azide (CH3N3), H2O, N2O and NO. In order to elucidate the mechanisms by which these observed products are formed, we carried out quantum mechanics calculations [CCSD(T)/M06-2X] for the possible reaction pathways. Based on these studies, we propose that the oxidation of MMH in an atmosphere of NO2 occurs via two mechanisms: (1) sequential H-abstraction and HONO formation, and (2) reaction of MMH with asymmetric ONONO2, leading to formation of methyl nitrate. These mechanisms successfully explain all intermediates observed experimentally. We conclude that the formation of asymmetric ONONO2 is assisted by an aerosol formed by HONO and MMH that provides a large surface area for ONONO2 to condense, leading to the generation of methyl nitrate. Thus we propose that the overall pre-ignition process involves both gas-phase and aerosol-phase reactions.

15. SUBJECT TERMS

16. SECURITY CLASSIFICATION OF:			17. LIMITATION OF ABSTRACT	18. NUMBER OF PAGES	19a. NAME OF RESPONSIBLE PERSON
a. REPORT **unclassified**	b. ABSTRACT **unclassified**	c. THIS PAGE **unclassified**	**Same as Report (SAR)**	**12**	

One major concern with the ARL MMH/RFNA mechanism is the lack of relevant experimental studies for its validation [6]. As part of an effort to provide experimental support for this mechanism, we investigated the pre-ignition reactions between MMH and HNO_3 (the major constituent of RFNA) in an earlier work [15]. These experimental results suggested that the current MMH/RFNA mechanism omits some important early reactions between MMH and HNO_3 and corresponding species. Since NO_2/N_2O_4 is another important constituent in RFNA, its early gas-phase reactions with MMH are examined in this work.

The current ARL mechanism for MMH/NTO, a subset of the MMH/RFNA mechanism, contains reactions categorized in two domains:

1. single-bond fission events to strip fragments from MMH and generate free radicals, and
2. radical–radical reactions to form either closed-shell or open-shell species.

Given the low temperature (<100 °C) in the pre-ignition environment, direct bond fission from MMH to produce H, CH_3 or NH_2 is unlikely so that NO_2 is the major free radical available initially. Based on this assumption, the ARL mechanism considers the two types of initial reactions:

1. H-abstraction from MMH and sequential HONO formations, and
2. recombination between NO_2 and MMH free radicals generated by H-abstraction.

However, these reactions do not fully explain the formation of a condensate that has been observed in several previous studies involving examinations of a residue from gas-phase reactions in a stoichiometric mixture of MMH and NO_2/N_2O_4 [16]. The IR properties of this residue are quite similar to the IR properties of a residue obtained from reactions between liquid-phase MMH and gaseous NO_2/N_2O_4 [17] The IR properties of the residue from these two studies suggest that monomethylhydrazinium nitrate ($MMH{\cdot}HNO_3$) is formed in addition to other species [16]. The formation of $MMH{\cdot}HNO_3$ was also detected by Saad et al. [18], who examined liquid-phase reactions between MMH and N_2O_4 in a system diluted by CCl_4 at −20 °C. In a recent work by Catoire et al. [13], it is suggested that the $MMH{\cdot}HNO_3$ detected as a major product in the residue by Semans et al. is not formed from reactions in the gas phase, since its elemental analysis matches rather poorly with that of the residue as determined by Breisacher et al. [19]. Catoire et al. suggests that nonionic compounds are formed and accumulate in a condensate. However, it appears that no experiments were carried out to confirm the formation of these nonionic compounds.

Based on the above discussion, there is a clear need to reexamine gas-phase reactions between MMH and NO_2/N_2O_4 at low temperatures in order to identify the relevant preignition products and reaction pathways. There are two objectives with the present work. First, we would like to experimentally identify *in situ* the species formed early in the preignition event from gas-phase reactions between MMH and NO_2/N_2O_4. Second, we would like to use quantum mechanics (QMs) tools to help elucidate the reaction pathways, since experimentally it is rather difficult to identify and quantify radicals, as well as to identify transition-state structures.

2. Methods

2.1. Chemicals

Monomethylhydrazine (MMH), purchased from Sigma–Aldrich and used without further purification, is a liquid with a concentration higher than 98%. Nitrogen dioxide (NO_2) is diluted in nitrogen (N_2) and stored in a pressurized cylinder. The mole concentration of NO_2 is 1%. In the gas phase, nitrogen dioxide and dinitrogen tetroxide always coexist due to the reversible dimerization reaction: $2NO_2 \leftrightarrow N_2O_4$ [20]. Since MMH and NO_2/N_2O_4 are highly toxic and corrosive, only small amounts of reactants were used in each test (i.e. ~0.2 μl MMH) and necessary protections (i.e., gloves, mask, etc.) were adopted.

2.2. Experimental setup and procedures

An overview of the experimental setup is shown in Fig. 1. The chamber reactor is made of stainless steel and has a 12 mm inner diameter and a path length of 65 mm. A thin layer of gold is coated on the chamber surface to minimize the potential of surface catalytic reactions. On each side of the cylindrical chamber is a ZnSe window for transmission of the modulated FT-IR beam from a Bruker IFS 66/S FT-IR spectrometer. $NO_2/N_2O_4/N_2$ mixture is injected into the chamber reactor through a Teflon tube, while MMH (~0.2 μl) is delivered by a 1 μl syringe. MMH is volatile (vapor pressure is 5 kPa at 20 °C) and evaporates rapidly upon injection. MMH vapor then mixes and reacts with NO_2/N_2O_4 in the chamber. The temporal evolution of IR-active species in the chamber, including initial reactants and products, is recorded by a time-resolved rapid scan on the FT-IR spectrometer. In each test a total of 390 spectra (the maximum memory limit), with a spectral resolution of 2.6 cm^{-1} and temporal resolution of 50 ms, are acquired. It should be noted that IR-inactive species such as N_2, O_2 and H_2, transparent to the IR beam, cannot be detected. Since the reactants are highly diluted in N_2 (~99%), the temperature and pressure variations in the chamber due to chemical reactions can be neglected.

Two types of tests, labeled as either oxidizer-rich or fuel-rich in the discussion below, were conducted.

- In the oxidizer-rich test, the reactor is purged with $NO_2/N_2O_4/N_2$ mixture and thus initially filled with the oxidizer. 0.2 μL MMH (3.8×10^{-6} mol) is quickly injected into the chamber and reacts with NO_2/N_2O_4.
- In the fuel-rich test, the chamber is purged with N_2 and 1 μL MMH (1.9×10^{-5} mol) is first injected into the chamber, which is then initially filled with MMH vapor and N_2. The mixture of oxidizers ($NO_2/N_2O_4/N_2$) is then pressurized into the chamber and reacts with MMH vapor upon mixing. The findings from these two types of tests are discussed separately in the results section.

Because residues may remain on the chamber wall after each test, the chamber wall is cleaned and conditioned through two steps before each new test. In the first step the chamber reactor

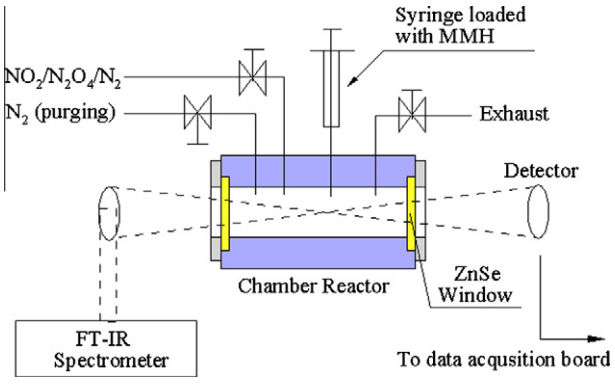

Fig. 1. A schematic view of the experimental setup.

is heated to about 350 °C by two embedded cartridge heaters. Most residues will either be gasified or decompose at this temperature, and therefore removed by the purge gas. In the second step the chamber wall is conditioned with NO_2/N_2O_4 or MMH vapor, depending on which one is introduced first. The conditioning is regarded complete when there is no noticeable decrease of NO_2/N_2O_4 (or MMH) in the closed chamber after a certain period of time.

2.3. Computational details

The geometry optimization and Hessian calculation were carried out at the level of M06-2X/6-311++G** [21]. The Hessian was used to provide the vibrational frequencies for zero-point energy (ZPE) and thermocorrections to enthalpy and entropy. In addition, at these optimized geometries we calculated the energy at the UCCSD(T)/6-31G** level of QM. In the reaction of HONO formation, the ONO-H distance is the key reaction coordinate and sensitive to different functionals. Comparing with geometries at transition state (TS) from CCSD/6-31+G** reported by McQuaid and Ishikawa [7], the greatest difference in O—H distance is at the TS of reaction to from CH_3NNH_2+HONO (2.170 v.s 1.908 Å), and for the remaining, the difference in O—H is less than 0.1 Å. These geometries differences, however, do not cause much difference in barrier heights of HONO formation, as shown in Section 4.1. All TS were shown to have exactly one negative eigenvalue by following the minimum energy path (MEP) scan to connect reactant and product. Free energies are reported at 298.15 K and 1 atm.

For reactions inside the aerosol or on the aerosol surface, we added the electrostatic interaction between reactants and surrounding ions with Poisson–Boltzmann solvation model (implicit solvent) implemented in Jaguar [22], using a dielectric constant of 80.37 and a spherical cavity of radius 1.40A for water. We consider that the solvation effects calculated for water represent the high dielectric properties expected for these systems, with the results depending little on the exact values as long as the dielectric constant is greater than 20 and radius smaller than 2.8A. All geometry optimizations, solvation and Hessian calculations were carried out with Jaguar 7.6 [23]. The UCCSD(T) calculation was done with NWChem [24,25].

3. Experimental results

3.1. Summary of spectroscopic data

Figures 2a, b and c show selected FT-IR spectra obtained from a typical test with the chamber initially filled with the oxidizer mixture ($NO_2/N_2O_4/N_2$); that is, the oxidizer-rich test. As shown in Fig. 2a, a chemical equilibrium is reached between NO_2 and N_2O_4. The equilibrium constant $K_p = P^2(NO_2)/P(N_2O_4)$ is about 0.1 atm at room temperature (20 °C) [26]. Therefore the initial mole composition of $NO_2/N_2O_4/N_2$ is about 0.855%/0.073%/99.072% at room temperature and 1 atmosphere in the chamber. After injecting 0.2 μl of MMH, the concentration of NO_2/N_2O_4 decreases and the products increase with time. Figures 2b and c show spectra acquired at $t = 7.5$ s and 15 s, respectively ($t = 0$ at MMH injection). The injection of the MMH takes a fraction of a second.

The original IR spectrum shown in Fig. 2c is a spectral summation of all IR-active species, including reactants and products. Most species can be readily distinguished by their characteristic vibrational frequencies. The identified species are labeled in Fig. 2c and their vibrational frequencies specified in Table 1. To identify other species in the product spectrum further spectral analysis was conducted by subtracting spectral bands of H_2O, NO_2, N_2O_4, N_2O, and CH_3ONO_2 with the remaining spectrum shown in Fig. 2d. Spectral subtraction is an important method to simplify the interpretation and analysis of the product spectrum [27]. For comparison, a spectrum of monomethylhydrazinium nitrate ($MMH{\cdot}HNO_3$), which was acquired in an earlier study on MMH/HNO_3 reactions, is shown in Fig. 2e. The broad spectral bands at 3322, 3080, 2796 and 2495 cm^{-1} in Fig. 2d match well with those in Fig. 2e, and these spectral bands were assigned to monomethylhydrazinium cation which may exist in three forms [15]: $[CH_3NHNH_3]^+$, $[CH_3NH_2NH_2]^+$ and $[CH_3NH_2NH_3]^{2+}$.

The spectral bands in the region 1000–1500 cm^{-1} do not match in Fig. 2d and e. In Fig. 2e, one band is centered at 1380 cm^{-1}, and it is typical for a nitrate salt [28,29]. In Fig. 2d, this band is centered at 1215 cm^{-1}, where many inorganic nitrite salts have a broad band [28–30]. Therefore, the broad spectral bands at 2400–3400 cm^{-1} and 1000–1500 cm^{-1} can be assigned to monomethylhydrazinium nitrite ($MMH{\cdot}HONO$). In addition, several spectral bands still exist in the region near 1600 cm^{-1} after subtracting bands attributed to NO_2. These remaining bands are primarily from nitromethane (CH_3NO_2) and methyl nitrite (CH_3ONO).

A summary of all identified IR-active species is given in Table 1, and the temporal evolution of the mole abundances of gaseous species is shown in Fig. 3. NO_2, H_2O, N_2O, and NO are quantified based on the HITRAN database [31]; HONO, CH_3N_3, CH_3ONO_2 and CH_3ONO are quantified based on data in the literature [32–35] on the gas-phase IR spectra of these species; CH_3NO_2 is quantified in this work by obtaining a reference IR spectrum after evaporating 0.2 μl liquid CH_3NO_2 (purchased from Sigma–Aldrich) into the same chamber which is introduced in Fig. 1, and the mole fraction of N_2O_4 is estimated based on the assumption that equilibrium is established quickly between NO_2 and N_2O_4 [26]. The aerosol product, monomethylhydrazinium nitrite, has not been quantified due to lack of reference calibration data. It should be noted that any significant amount of MMH has not been detected in any of the 390 spectra acquired, which suggests that either the chemical reaction rate of MMH with NO_2/N_2O_4 is much faster than the evaporation rate of MMH liquid, or that the tip of the needle on the syringe used for injection does not penetrate any portion of the volume of the modulated beam of the FTIR spectrometer, or both. By carefully examining the acquired spectra shown in Fig. 2b–d, the Q-branch of several bands attributed to MMH can be detected, however.

Figure 4a–c shows selected FT-IR spectra obtained from a typical test with the chamber initially filled with 5.8% (molar basis) MMH vapor and 94.2% N_2. The spectrum of MMH acquired before introducing NO_2/N_2O_4 is shown in Fig. 4a and detailed assignments of MMH vibrations are provided in previous work [15]. Figure 4b shows the spectrum acquired at the moment when $NO_2/N_2O_4/N_2$ mixture is injected into the chamber, and Fig. 4c shows the last spectrum acquired in the test. Figure 4d is acquired by subtracting the IR spectral bands of MMH and NO_2 from Fig. 4c. The dominant species identified in Fig. 4d include monomethylhydrazinium nitrite and methyl diazene ($CH_3N{=}NH$). Very small amounts of N_2O, CH_3N_3 and CH_3ONO_2 were also identified. A summary of these identified species and their major IR frequencies are given in Table 1.

It is generally believed that the first step in reactions between MMH and NO_2 is direct H-atom abstraction by NO_2 leading to formation of HONO and a methylhydrazyl radical (CH_3NHNH or CH_3NNH_2) [13,36]. This is supported by our observation of HONO formation:

$$CH_3NHNH_2 + NO_2 \rightarrow CH_3NNH_2 \text{ (or } CH_3NHNH) + HONO \quad (1)$$

The methylhydrazyl radical can further react with NO_2 with potential pathways discussed by Catoire et al. [13] and Ishikawa and McQuaid [9]. Catoire et al. suggested that $CH_3N(NO_2)NH_2$ and $CH_3N(ONO)NH_2$ are the major stable pre-ignition products which account for the formation of a white-yellow condensate [43]. However, these species have not been identified as major early species in

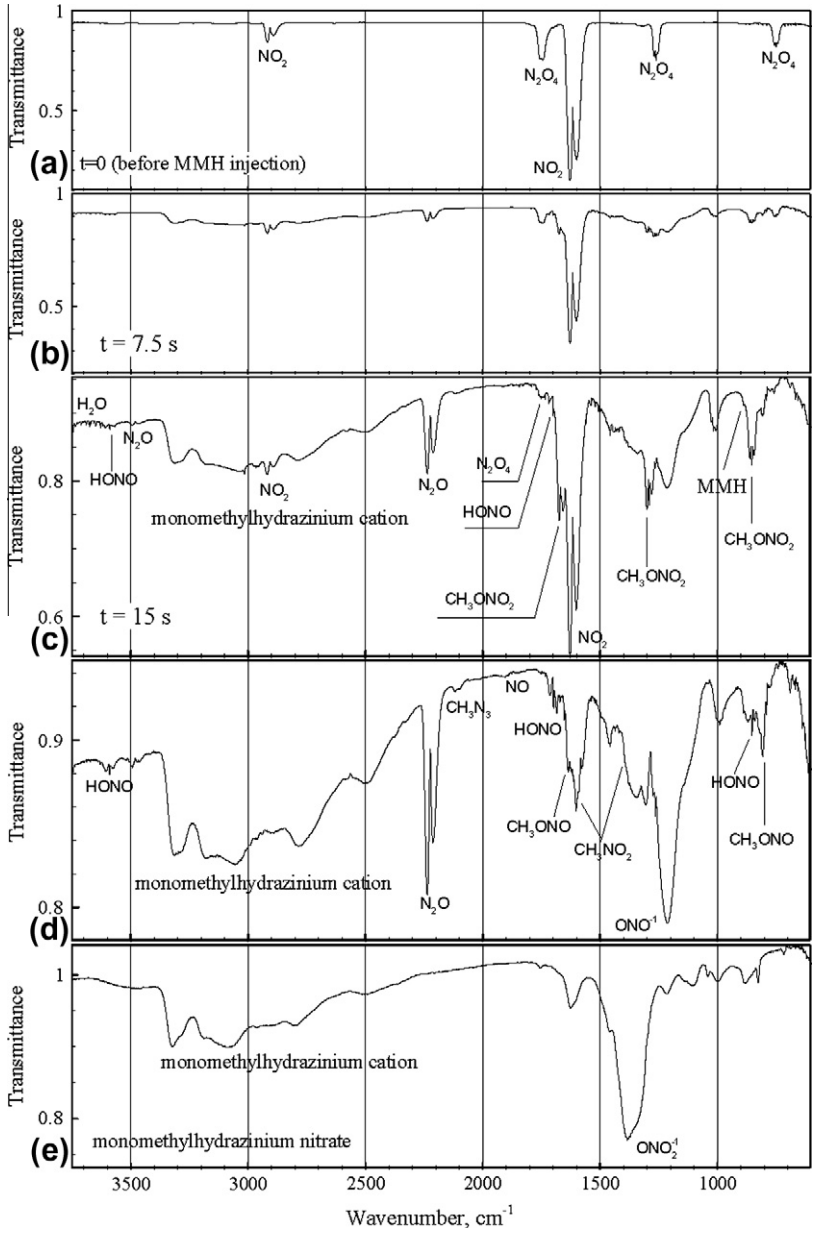

Fig. 2. Selected IR spectra from a typical oxidizer-rich test with NO_2/N_2O_4: (a) IR spectrum of NO_2/N_2O_4 mixture acquired before injecting MMH, (b) IR spectrum acquired at t = 7.5 s after injecting MMH, (c) IR spectrum acquired at t = 15 s after injecting MMH, (d) IR spectrum obtained by subtracting H_2O, NO_2, N_2O_4, N_2O and CH_3ONO_2 from the IR spectrum in (c), and (e) IR spectrum of monomethylhydrazinium nitrate acquired in an early work [15].

Table 1
IR frequencies of species discussed in this work (vs = very strong, s = strong, m = medium).

Species	Major IR bands observed in this work (cm^{-1})	Refs.
Reactants:		
MMH	3261(s), 2960(vs), 2852(vs), 2785(vs), 1595(m), 1480(s), 1451(s), 1293(m), 1119(s), 968(s), 888(vs), 771(vs)	[37]
NO_2	2907(m), 1617(vs)	[38]
N_2O_4	1750(s), 1261(s), 749(s)	[39]
Products:		
MMH Nitrite	3310(s), 3180(s), 3050(s), 2778(s), 2495(m), 1325(s), 1213(vs), 990(m)	
trans-HONO	3590(m), 1699(s), 1264(s), 791(s)	[40]
cis-HONO	1640(s), 853(s)	[40]
$CH_3N{=}NH$	3125(m), 2988(m), 2924(m), 1457(m), 1140(m), 844(s)	[41]
CH_3N_3	2190(m), 2107(s), 1276(m)	[33]
CH_3ONO_2	2965(m), 1666(vs), 1435(m), 1290(vs), 1017(s), 855(s), 759(m), 660(m)	[34]
CH_3ONO	1678(s), 1620(vs), 991(s), 811(vs)	[35]
CH_3NO_2	1583(s), 1397(s), 1378(s)	[42]
H_2O, NO, N_2O	See HITRAN database	[38]

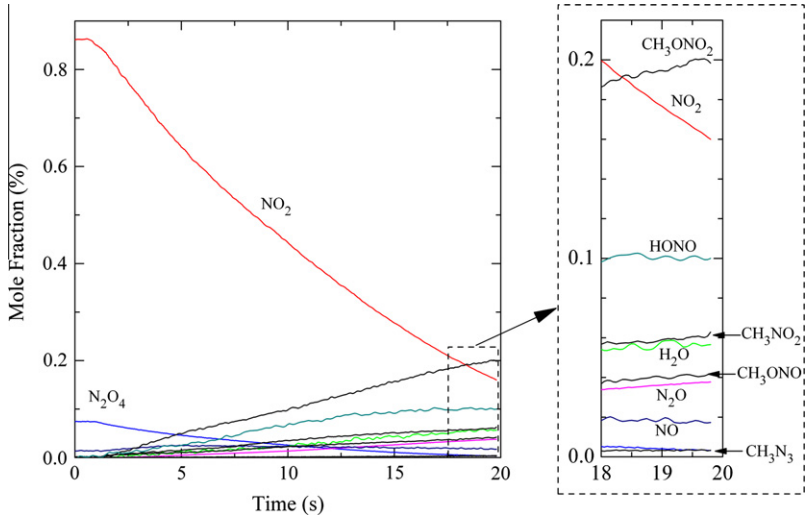

Fig. 3. Temporal evolution of the mole abundances of gaseous species when 0.2 μl MMH was injected into the chamber reactor and reacted with NO_2/N_2O_4 in 1 atm N_2 (*Note*: the aerosol product, MMH·HONO, is not shown in this plot since it has not been quantified in this work).

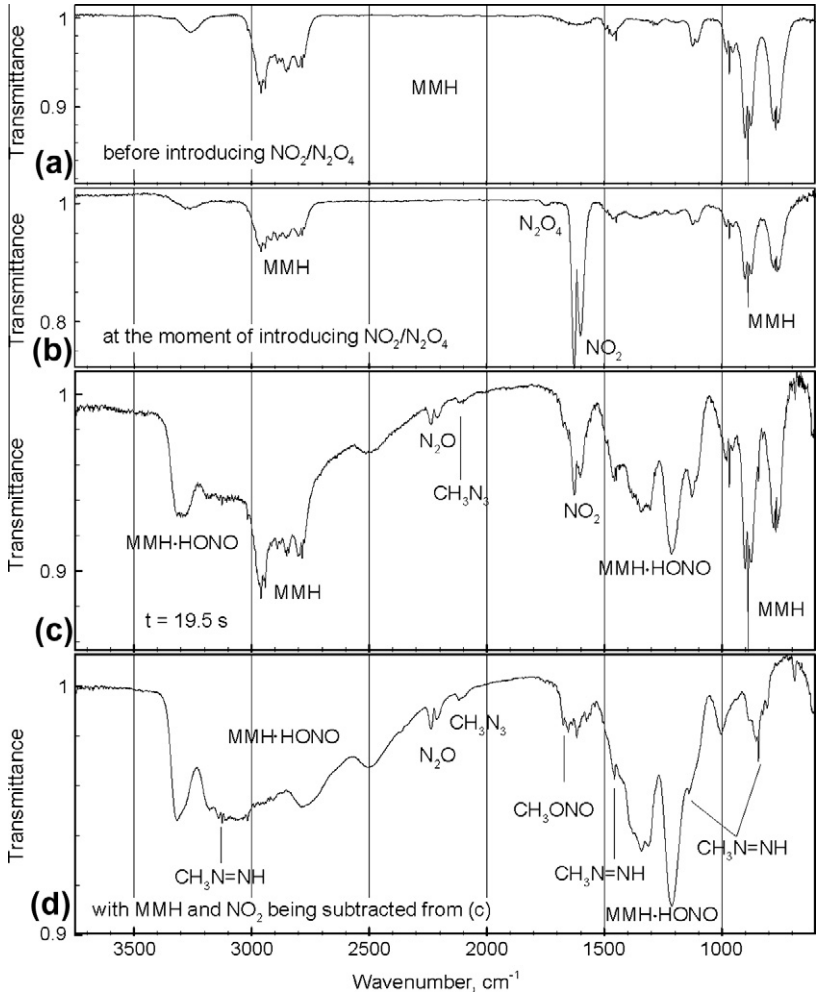

Fig. 4. Selected IR spectra from a typical test with MMH injected first; that is, the fuel-rich case: (a) IR spectrum of MMH vapor acquired before introducing the oxidizer, (b) IR spectrum acquired at the moment of introducing $NO_2/N_2O_4/N_2$ mixture, (c) IR spectrum acquired at t = 19.5 s and (d) IR spectrum obtained by subtracting MMH and NO_2 from the IR spectrum in Fig. 4c.

the present work. Based on thermochemical calculations, Ishikawa and McQuaid [9] suggested alternative pathways of direct H atom abstraction from the methylhydrazyl radical by NO_2 leading to the formation of methyl diazene ($CH_3N{=}NH$) or $CH_2{=}NNH_2$. We ob-

serve $CH_3N{=}NH$ only as a major product (Fig. 4d), and therefore we conclude that the likely reaction between methylhydrazyl radical and NO_2 is HONO elimination with the formation of methyl diazene ($CH_3N{=}NH$).

$$CH_3NNH_2\ (\text{or } CH_3NHNH) + NO_2 \rightarrow CH_3N=NH + HONO \quad (2)$$

It should be noted that with excess NO_2, $CH_3N{=}NH$ can be rapidly oxidized [13], and is not detected in Fig. 2.

3.2. Aerosol formation

In previous studies [16,43], a large amount of condensate was observed when mixing gaseous MMH and NO_2. The condensate was collected and examined ex situ with IR spectroscopic techniques to reveal it contained monomethylhydrazinium nitrate in addition to other species. Similar findings were observed in reactions between liquid-phase MMH and gaseous NO_2 by Mayer et al. [17] In liquid-phase reactions between MMH and N_2O_4 diluted by CCl_4, Saad et al. identified many different products, including methanol, methylamine, dimethylamine, methylnitrosamine, dimethylnitrosamine and N-methylformamide in addition to $MMH{\cdot}HNO_3$ [18]. These findings from Saad et al. suggest that the reaction pathways in the liquid phase are quite different than those in the gas phase, as indicated by the species identification in Figs. 2 and 4. Similar to the results by Seamans et al. [16], we also observe an *in situ* formation of a condensate (fog) when MMH vapor reacts with $NO_2/N_2O_4/N_2$ mixture. This observation is from a separate test in which the two reactants were introduced into a transparent plastic chamber. An *in situ* condensate formation can also be inferred from changes in the baseline slope in the IR spectra in Fig. 2, and Kravets et al. [44] present an excellent discussion on the effect of small particles on spectral transmittance. The IR transmittance decreases with increasing wavenumber due to the Rayleigh scattering of small particles which generates a baseline slope in the IR spectra.A preliminary analysis of the condensate by Seamans et al. [16] indicated a mass composition of C: 14.6%, H: 8.1%, N: 46.4%, and O: 30.9% (by difference). Catoire et al. [13] suggested that the monomethylhydrazinium nitrate is not likely formed in gas-phase reactions. Instead Catoire et al. attributed this condensate to covalently bonded nitro and nitrite compounds produced from methylhydrazyl radical and NO_2 because these species have calculated a mass composition of C: 13.2; H: 5.5; N: 46.1 and O: 35.1, consistent with the analysis of Seamans et al. [16] Our *in situ* IR analysis reveals that this condensate is mainly composed of an ionic monomethylhydrazinium nitrite salt ($MMH{\cdot}HONO$). This nitrite salt has a calculated mass composition of C: 12.9; H: 7.5; N: 45.2 and O: 34.4, also in agreement with Seaman's analysis. Based on HONO as a weak acid [45] ($pK_a = 3.16$) and MMH as a well-known base [46] ($pK_a = 8.1$), formation of monomethylhydrazinium nitrite through an acid–base proton transfer reaction is very likely. The gas-phase acid–base reaction has been thoroughly investigated by atmospheric chemists, [47–50] and it is generally believed that a hydrogen-bonded neutral complex is formed prior to the occurrence of proton transfer. This type of reaction is widely known as 'gas-to-aerosol' or 'gas-to-particle' reaction because an aerosol of salts is usually formed.

$$CH_3NHNH_2 + HONO \rightarrow CH_3NHNH_2\cdots H\cdots ONO \rightarrow [CH_3NHNH_3^+ \cdot ONO^-] \quad (3)$$

$$[CH_3NHNH_3^+ \cdot ONO^-]_{n-1} + [CH_3NHNH_3^+ \cdot ONO-] \rightarrow [CH_3NHNH_3^+ \cdot ONO^-]_n \quad (4)$$

Seamans et al. [16] found that the amount of such condensate was more than 20% by weight of the total reactants in some experiments. Therefore, reactions (3) and (4) must be included in the MMH/RFNA mechanism. Furthermore, the condensate formation can play an important role in the ignition event for several reasons. First, the associated proton transfer is quite exothermic, thus providing energy for increase in temperature of the system and energy for the endothermic H-abstraction reactions forming HONO. Second, we consider that the formed particle provide a suitable medium for enhanced surface reactions. Third and finally, as molecules become "trapped" in a condensed phase, the concentration of gaseous species, such as MMH, NO_2 and HONO, is likely to be increased leading to increased reaction rates.

3.3. Comparison between fuel-rich and oxidizer-rich conditions

Under fuel-rich conditions, shown in Fig. 4, reactions (1)–(4) are relevant. With excess MMH, HONO formed by reaction (1) and (2) can be almost fully consumed by reaction (3) to form $MMH{\cdot}HONO$. The amount of gaseous HONO in all spectra is almost unnoticeable due to the high concentration of MMH driving the salt formation with HONO. Methyl diazene formed by reaction (2) is one of the final products with excess MMH shown in Fig. 4.

Under oxidizer-rich conditions, methyl diazene ($CH_3N{=}NH$) is further oxidized and barely detected, as indicated in Fig. 2. Based on IR analysis subsequent reactions between $CH_3N{=}NH$ and NO_2 produces large amounts of CH_3ONO and CH_3NO_2. The first step is the likely H-atom abstraction by NO_2 leading to the formation of methyl diazene radical $CH_3N{=}N{\cdot}$and HONO. The possible reactions between $CH_3N{=}NH$ and NO_2 under oxidizer-rich conditions are:

$$CH_3N=NH + NO_2 \rightarrow CH_3N=N^{\cdot} + HONO \quad (5)$$

$$CH_3N=N^{\cdot} \rightarrow CH_3^{\cdot} + N_2 \quad (6)$$

$$CH_3^{\cdot} + NO_2 \rightarrow CH_3NO_2\ (\text{or } CH_3ONO) \quad (7)$$

4. Theoretical results

4.1. H-atom abstraction from MMH

The oxidation of MMH via sequential HONO formation and the final N_2 generation were studied computationally as shown in Scheme 1. The first H-abstraction from MMH has been studied in detail by McQuaid and Ishikawa [7]. Their reported barrier heights for H-abstractions from three different positions (H on N-CH_3 and two H on N-NCH_3 – *cis* and *trans* to the methyl group, respectively) to form *cis*-HONO are 10.1, 10.6 and 11.2 kcal/mol (without ZPE or thermocorrections) at CCSD(T)/6-311+G(2df,p)//CCSD/6-31+G(d,p) level relative to free NO_2 and MMH.

These results are close to our values of 8.0, 9.8 and 10.3 kcal/mol (including ZPE and temperature corrections, relative to free NO_2 and MMH). We find that the most readily abstracted H-atom is from the nitrogen with the methyl group, in agreement with the previous study. The binding energy between the product HONO and the free radical is substantial (10–13 kcal/mol enthalpy), reducing the free energy of the post-reaction complex to even lower levels than the unbound free radicals GInt1 – GInt3. However in normal experimental conditions the partial pressure of HONO is usually much lower than 1 atm (the reference state), favoring the formation of unbound free radicals, after taking concentration correction into account. The interconversion between GInt2 and GInt3 via N—N bond rotation has a high barrier (~29 kcal/mol) because the N—N bond has some double-bond character due to the delocalization of the N lone pair. Abstraction of an H atom from a methyl group (GTS4) is ~10 kcal/mol higher in energy than from N atoms. Furthermore, this reaction is 16.1 kcal/mol endothermic, in contrast to H-abstractions from N atoms, which are almost thermoneutral. Therefore

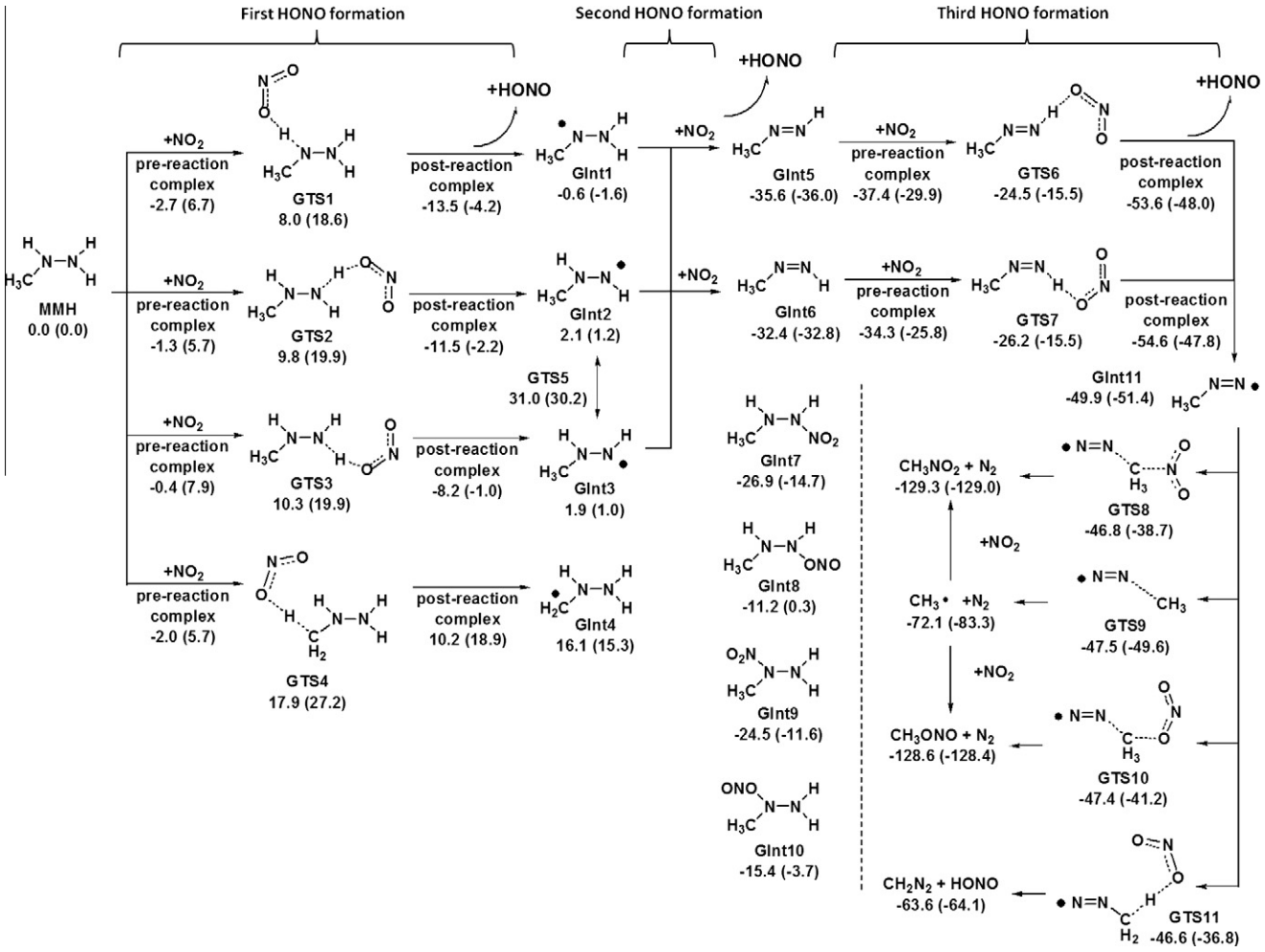

Scheme 1. Reactions between MMH and NO_2 in gas phase. Barriers of all H-abstractions from N of MMH to form HONO are about 10 kcal/mol, and the same H-abstraction from methyl group is 16.1 kcal/mol endothermic and has ~10 kcal/mol higher barrier, rendering the oxidation of carbon slower at low temperature. Enthalpies and Gibbs free energies (in the parentheses) are calculated at 298.15 K and 1 atm. *cis*-HONO at standard state is used as reference product.

H-atom abstraction from the methyl group will not play an important role during the pre-ignition event, and experimentally we observed abundant methyl-containing compounds, indicating the inertness of methyl group at room temperature. Consequently reactions beyond GInt4 are not considered in Scheme 1.

4.2. H-atom abstraction from CH_3NNH_2 or CH_3NHNH

The H-abstraction reactions from either CH_3NNH_2 or CH_3NHNH very likely have no barrier because of stabilization of the N *p* orbital bonded to the H with delocalization of the adjacent N lone pair. Indeed we could not find a transition state in the electronic energy surface despite an exhaustive search. The free energy surface after including ZPE might well lead to a barrier. Ishikawa and McQuaid [9], using the MPWB1 K functional, found that 1–2 kcal/mol of kinetic energy is enough to activate H-atom abstraction, indicating very low barriers for H-abstraction. GInt7 – GInt10 are products from recombination between two radicals (GInt1 – GInt3 and NO_2). All of them are enthalpically and entropically less stable than the product of HONO formation, GInt5 and GInt6. These recombination products are not detected in our experiment, where MMH and NO_2 are in gas phase diluted with N_2., With higher concentration of MMH and NO_2 or reacting in liquid phase will change free energy profile, making the recombination products more favorable.

4.3. H-atom abstraction from $CH_3N{=}NH$

The enthalpic barrier for the H-atom abstraction is 11.1 kcal/mol for anti-$CH_3N{=}NH$ (GInt5 → GTS6 → GInt11) and 6.2 kcal/mol for syn-$CH_3N{=}NH$ (GInt6 → GTS7 → GInt11). The $CH_3N{=}N$ radical (GInt11) can either break the C—N bond to release N_2 and CH_3 radical via TS9 (ARL mechanism reaction No. 456) with only 2.4 kcal/mol barrier, or undergo NO_2 attack at different orientations to form CH_3NO_2 and CH_3ONO via TS8 and TS10 with barrier heights 2.5 and 3.1 kcal/mol, respectively.

It is not likely that the free radicals CH_3 and CH_3NN play a significant role in the formation of CH_3ONO_2. NO_2 is much more abundant than $ONONO_2$ in the gas phase (see Section 4.5), therefore the recombination of CH_3 or CH_3NN with NO_2 to give CH_3NO_2 or CH_3ONO should be much faster than the recombination of CH_3 or CH_3NN with $ONONO_2$. The other pathway to form CH_3ONO_2 is via the recombination of NO_2 with the CH_3O radical, which is generated from the reaction $CH_3{+}NO_2 \rightarrow CH_3O{+}NO$; however, this reaction cannot fully explain the production of CH_3ONO_2 either due to the much different concentrations of NO and CH_3ONO_2. In addition, the formation of CH_2N_2 via H-abstraction from methyl group is also found to have a low barrier (3.3 kcal/mol). However this product was not detected experimentally, indicating that the direct dissociation of methyl free radical from GInt11 may be much faster than other bimolecular pathways.

4.4. Formation of MMH·HONO aerosol and its lower reactivity

In each step of Scheme 1, HONO is produced, which is able to form aerosol with unreacted MMH because the basic N atoms on MMH are able to accept a proton from HONO. As shown in Scheme 2, protons in MMH·HONO complexes in gas phase prefer to stay on HONO. The enthalpies to form *n*HONO·MMH complexes (n = 1, 2) are roughly additive (−21.5 kcal/mol from the sum of enthalpy of GInt12 and 13 vs. −18.9 kcal/mol of GInt14) and the free energies to form these complexes are about thermoneutral (−2.1, 0.1 and 0.7 kcal/mol for GInt12, GInt13 and GInt14). In the strong solvation environment (in the aerosol), the proton transfer from HONO to MMH is more favored and exothermic, which accounts for the observation of ONO^- anion in the IR spectra. However, the reaction heat to transfer one and two protons from the MMH·2HONO complex in a solvated system differ little (5.7 vs. 8.0 kcal/mol exothermic), unlike complexes in the gas phase. It is because in solvated system the electrostatic repulsion between two positively charged N centers partially cancels the energy gain from the neutralization. Hence, the pathways for continued growth and composition of the aerosol can be either $MMH^{2+}\cdot 2ONO^-$ or $MMH^+\cdot ONO^-$. In the oxidizer-rich case, however, the former composition is more likely. The spontaneous nucleation in gas phase followed by the exothermic growth make the aerosol formation a rapid process as observed in the experiment.

We also found that the MMH·HONO aerosol is less reactive than free MMH. Reactions to abstract H from MMH·HONO complex have barriers 7–9 kcal/mol higher than the same H-abstraction from MMH. The reason is that in free MMH, the lone pairs on the N can stabilize the transition state via resonance, whereas such stabilization is less available when lone pairs donate electron density to the proton, resulting in a higher barrier. The increase of the barrier for HONO formation resulting from the salt formation was also observed in the case of alkylamine and nitric acid [51]. As a result, growth of the particles is favored over H-abstraction reactions at the low temperatures of our experiments. As the temperature increases, particles will either undergo H-abstraction reactions or evaporate into MMH and HONO so that particles will shrink and eventually disappear. Such a phenomenon of particle disappearance is observed just prior to ignition in the MMH·HNO3 reaction system [15].

4.5. Reactions of asymmetric dimer of NO_2, $ONONO_2$ in gas phase

The formation of ONO_2^- and CH_3ONO_2 cannot be explained by simple H-atom abstractions or recombination of the radical intermediates with NO_2. One potential source of nitrate is from the isomerization of N_2O_4. It is known that liquid NO_2 dimerizes to form N_2O_4 and disproportionates into NO^+ and NO_3^- [52]. NO_2 can also react with water vapor to give HONO and HNO_3. Finlayson-Pitts and coworkers [53] proposed that the asymmetric isomer $ONONO_2$ is the key intermediate as the source of nitrate. Our previous study shows that the reaction to form $ONONO_2$ has low enthalpic barrier (<5 kcal/mol) [54], which means equilibrium between NO_2 and $ONONO_2$ is very fast. Recently Lai et al. [55] also found that $ONONO_2$ can play an important role in the hypergolic

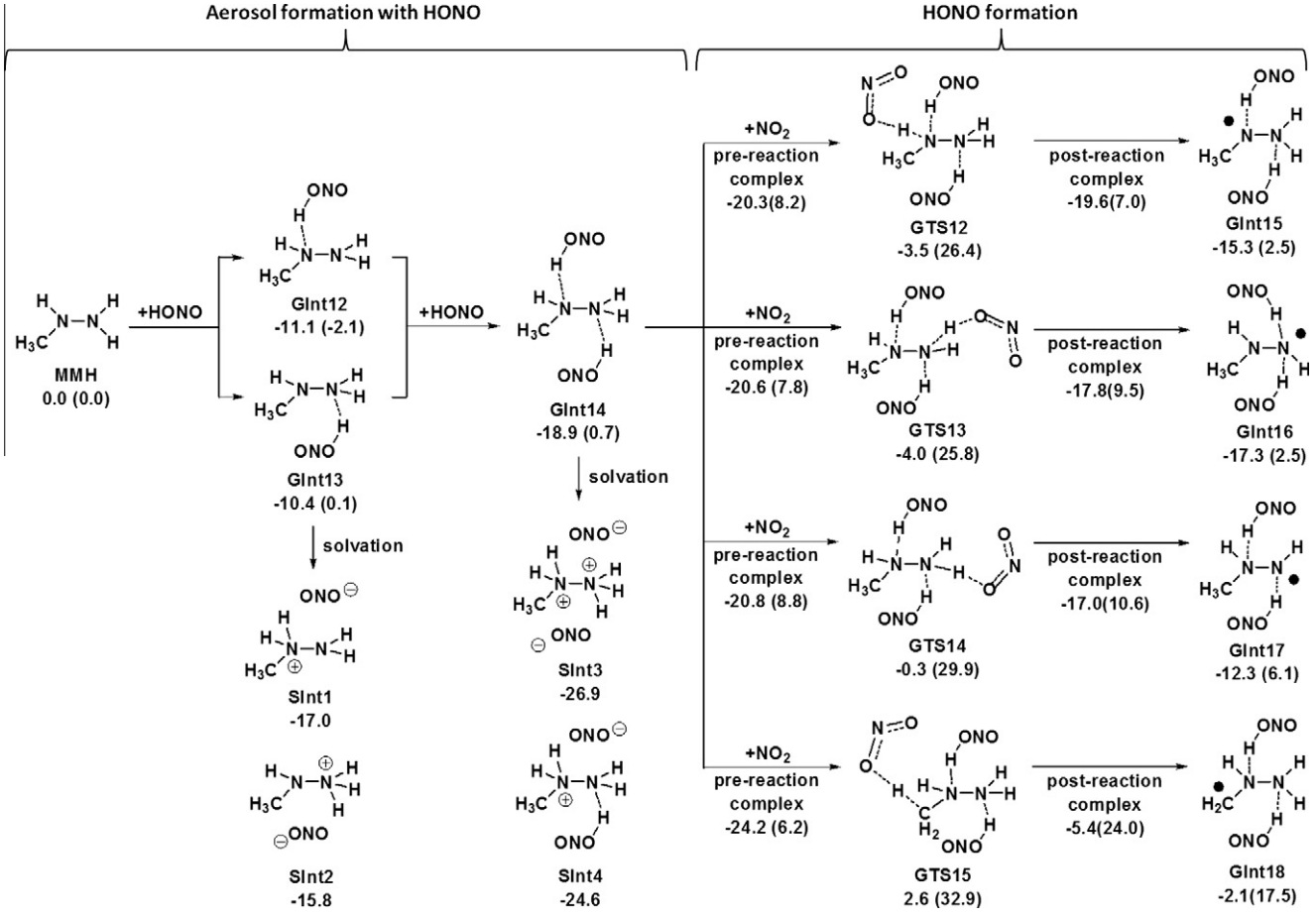

Scheme 2. The formation of aerosol MMH·HONO and MMH·2HONO followed by H-abstraction and HONO formation. The barriers of H-abstraction from MMH·2HONO aerosol are 7–9 kcal/mol higher than the ones from MMH. Enthalpies and Gibbs free energies (in the parentheses) are calculated at 298.15 K and 1 atm. *cis*-HONO at standard state is used as reference product.

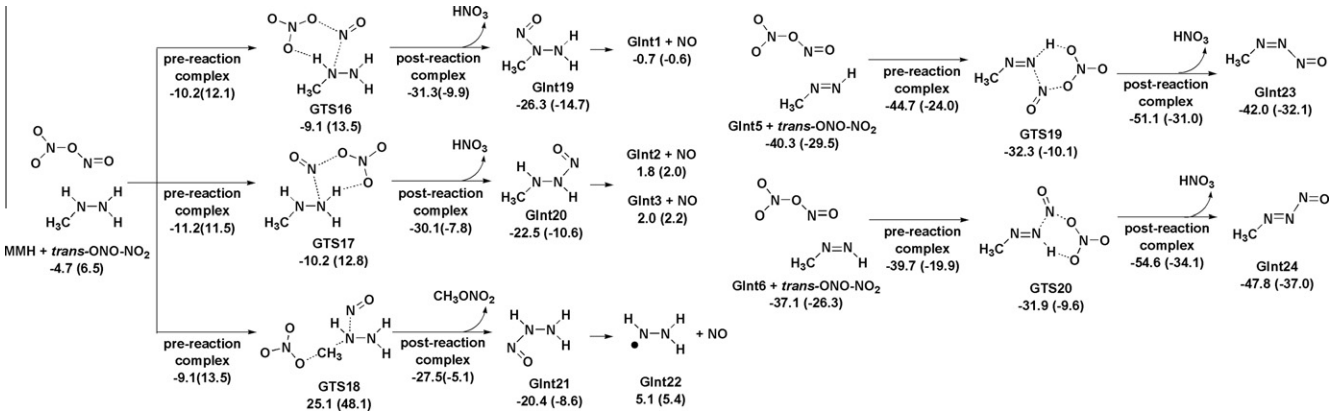

Scheme 3. The reactions between $ONONO_2$, MMH, Gint5 and Gint6 in gas phase. These reactions have low barriers and produce HNO_3 as the source of nitrate anion observed experimentally. Enthalpies and Gibbs free energies (in the parentheses) are calculated at 298.15 K and 1 atm. *cis*-HONO at standard state is used as reference product.

reaction between hydrazine and liquid NTO. We would also like to check if $ONONO_2$ plays the similar role in the gas phase reaction between MMH and NO_2.

The easiest reactions between MMH and trans-$ONONO_2$ is the new N—N bond formation between NO^+ and electron-rich N atoms on MMH followed by the proton transfer from N—H bond to NO_3^- to form nitric acid, as shown in Scheme 3. Although it is very easy to form nitric acid (enthalpic barrier is about 1 kcal/mol), to form methyl nitrate is difficult in gas phase (34 kcal/mol enthalpic barrier) due to the unfavorable charge separation (nitrate anion has to attack from the back of methyl group, which is far from the positive N center). Therefore, the gas phase reactions between MMH and $ONONO_2$ can easily generate HNO_3 and explain the experimental observation of NO_3^-, however, they cannot explain the abundant CH_3ONO_2 observed in the IR spectrum, which we surmised to be produced on the surface of aerosol, as studied in the Section 4.6.

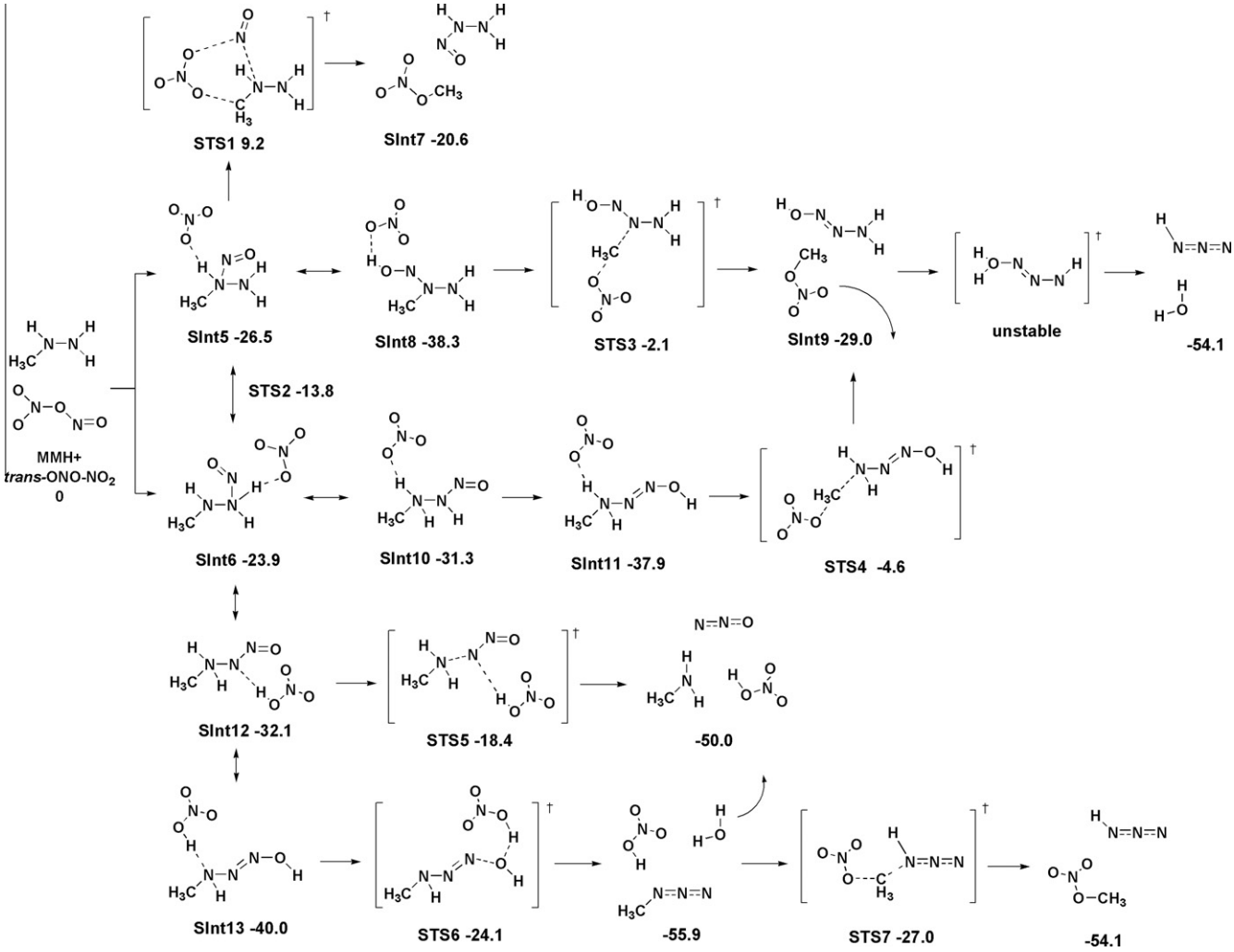

Scheme 4. The reactions between $ONONO_2$ and MMH in water to simulate potential energy surface in the aerosol. Enthalpies are calculated at 298.15 K and 1 atm. Several gas products, such as CH_3ONO_2 and N_2O, can desorb from the aerosol and be observed via IR spectra.

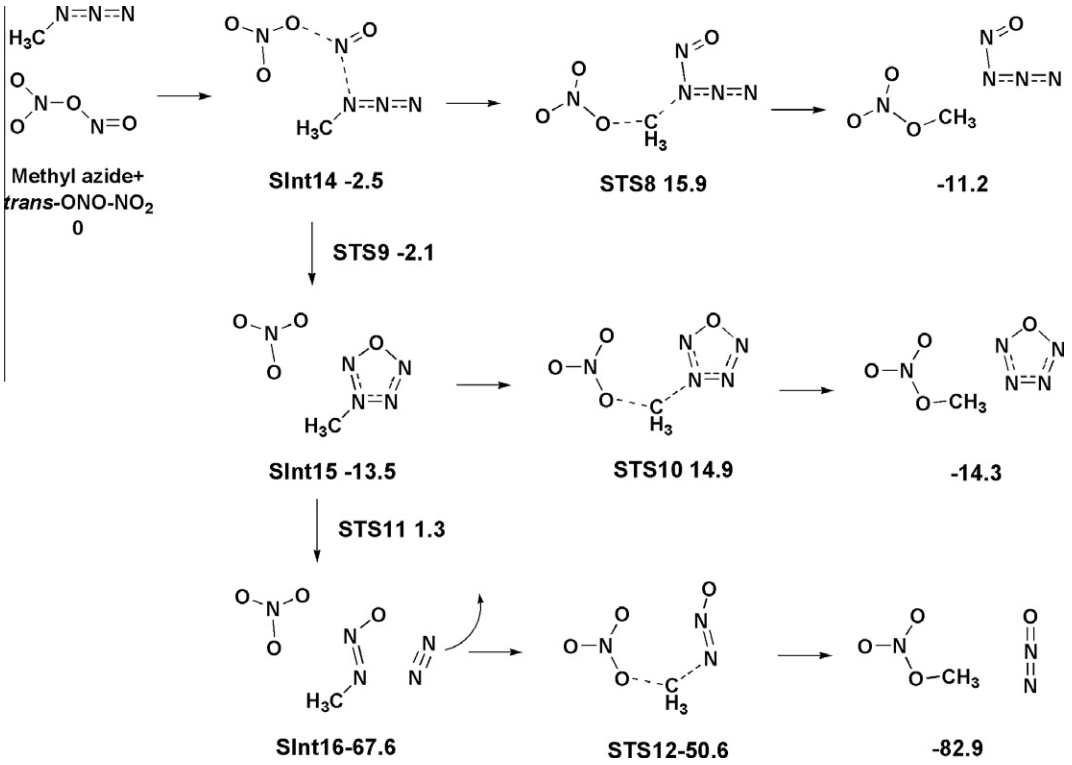

Scheme 5. The reactions between CH_3N_3 and $ONONO_2$ in water to simulate potential energy surface in the aerosol. The reaction path via SInt14, SInt15, SInt16 and STS12 has low barriers to form CH_3ONO_2. Enthalpies are calculated at 298.15 K and 1 atm.

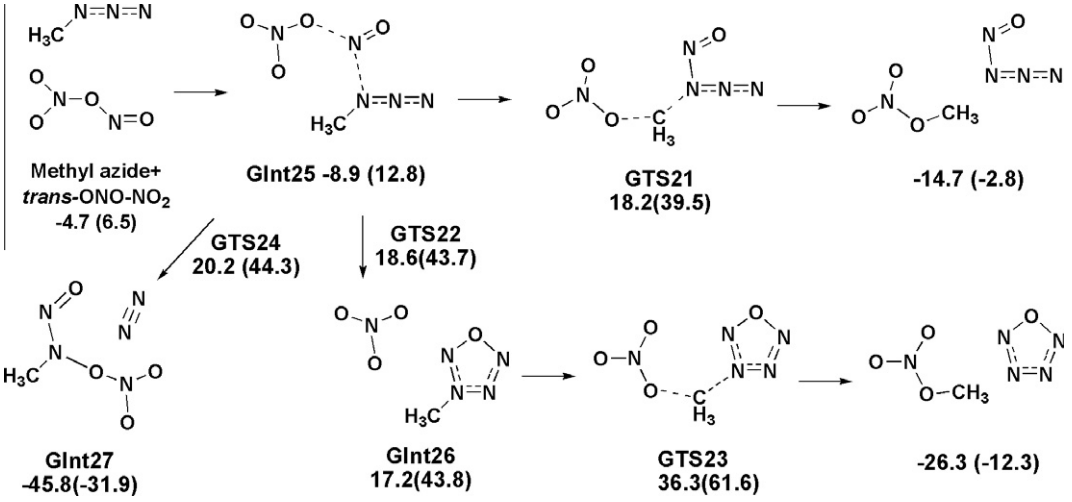

Scheme 6. The reactions between CH_3N_3 and $ONONO_2$ in gas phase. All barriers are significantly higher than the corresponding reactions in water, indicating the importance of solvation effect. Enthalpies and Gibbs free energies (in the parentheses) are calculated at 298.15 K and 1 atm.

$ONONO_2$ can also react with intermediates from HONO formation, such as GInt5 and GInt6, as shown in Scheme 3. N atoms on GInt5 and GInt6 are sp^2 hybridized, not as electron-rich as the sp^3 hybridized ones, therefore barriers to abstract H from GInt5 and GInt6 to form HNO_3 are about 10 kcal/mol higher than H-abstractions from MMH.

4.6. Reactions facilitated by aerosol to form CH_3ONO_2

Several experiments indicate that NO_2 can react with water or alcohol heterogeneously (surface-catalyzed) [53,56–58], probably via the same $ONONO_2$ intermediate [53]. The aerosol of ONO^- and MMH cation (such as Sint1-Sint4) provides polar ionic surface that can stabilize the asymmetric $ONONO_2$ and promote nitrate formation. This pathway can be favored at higher NO_2 concentrations because $ONONO_2$ concentration is proportional to $[NO_2]^2$, which also explain the experimental observation that the formation of methyl nitrate was only observed in the NO_2-rich atomsphere. Because asymmetric $ONONO_2$ has high dipole moments (3.45D for *cis* and 2.96D for *trans* at B3LYP/6311G*+ level) [54] we expect the concentration of $ONONO_2$ to be greatly increased if it is absorbed on a polar surface or formed a molecular complex with a polar molecule.

To study reactions between $ONONO_2$ and MMH on the polar surface or the sub-surface of the aerosol, we used an implicit solvation model to include the interaction between reactants and

surrounding ions. Our proposed reaction mechanism between MMH and $ONONO_2$ and the corresponding enthalpies are shown in Scheme 4.

In solution phase, $ONONO_2$ has strong tendency to dissociate into NO_3^- and NO^+ with the presence of electron-rich MMH. The electron-deficient NO^+ makes N—N bond with the electron-rich N, preferably the methyl substituted N, on MMH to form SInt5 and SInt6. From SInt5, nitrate anion can attack from the back methyl group to form methyl nitrate with 35.7 kcal/mol barrier.

Once the N—N bond is formed, the acidity of the adjacent N-H bond increases and the overall complex is similar to the salt generated from the neutralization between HNO_3 and corresponding amine. We assumed that the proton transfer in such a polar environment has a low barrier. Therefore to study tautomers as intermediates is enough to depict the potential energy surface. In our calculations, these tautomers are tightly constrained to conserve the number of protons, while in aerosol protons can exchange with the environment, implying our barriers should be the upper bounds of true barriers.

Even with free nitrate anion in aerosol, the barriers for the nucleophilic substitution of the methyl group on MMH are considerable. Among several possible tautomers, SInt8 and SInt11 are the easiest two to form CH_3ONO_2 via STS3 and STS4 to SInt9, with barriers 36.2 and 33.3 kcal/mol, respectively, giving the final products, hydrazoic acid and water. See SI for other tautomers and corresponding TS to form CH_3ONO_2. It is also possible to form N_2O and methyl amine by breaking the N—N bond in SInt12 via STS5 with 13.7 kcal/mol barrier, corresponding to the experimental observation of N_2O.

An easier path to form CH_3ONO_2 involves the intermediate CH_3N_3 formed via STS6 with 15.9 kcal/mol enthalpic barrier. As shown in Scheme 5, in solution phase, CH_3N_3 prefers to react with $ONONO_2$ to form a 5-member ring intermediate (SInt15) with negligible barrier, which then decomposes to release N_2 with 14.8 kcal/mol barrier, and the product (SInt16) undergoes nucleophlic attack of nitrate to form CH_3ONO_2 and N_2O with 17.0 kcal/mol enthalpic barrier and 32.3 kcal/mol exothermicity. This mechanism fits to the fact that azide reacts completely with NOCl or N_2O_4 in condense phase to give nitrate, N_2O and N_2 [59,60], and was proposed in Ref. [18]. The 5-member ring intermediate and its decomposition pathway have also been reported [61].

The solvation effect plays an important role in facilitating the decomposition of CH_3N_3, because in gas phase, similar reactions to produce CH_3ONO_2 have enthalpic barriers higher than 25 kcal/mol, as shown in scheme 6. In gas phase, to form the same 5-member ring intermediate via GTS22 has a 27.5 kcal/mol enthalpic barrier, The STS11-like transition state, GTS24, does not connect to a 5-member ring intermediate in the MEP scan, instead it leads to the path to dissociate N_2 from CH_3N_3 directly, with barrier height 29.1 kcal/mol. These reaction paths do not lead to rapid production of CH_3ONO_2, leading to the conclusion that the formation of CH_3N_3 and CH_3ONO_2 take place on the surface of aerosol but not in gas phase.

Once N_2O, CH_3ONO_2, and CH_3N_3 are formed on the surface of aerosol, they can desorb and drive reactions further towards completion. The energetics is favorable due to the partial oxidation of MMH. Also the exchange between gas phase and aerosol species is plausible – NO_2 can be absorbed onto the aerosol surface and oxidize intermediates shown in Scheme 2, leading to a complicated multiphase picture of pre-ignition reactions.

5. Conclusions

We studied reactions between MMH and NO_2 vapor in a gold-coated chamber reactor with Fourier transform infrared spectrometry at both MMH-rich and NO_2-rich conditions. At low concentration of NO_2 the major products are MMH·HONO and $CH_3N{=}NH$ and the minor products are N_2O, CH_3N_3, CH_3NO_2 and CH_3ONO. Our QM calculations elucidate possible mechanisms of H-abstraction by NO_2 from MMH to form HONO, which then forms condensate by reacting with MMH in fuel-rich condition. We find that $CH_3N{=}NH$ is formed after a second H-abstraction from MMH. Further H-abstraction produces CH_3ONO, CH_3NO_2 and N_2. At higher concentrations of NO_2 the major products are monomethylhydrazinium nitrite and methyl nitrate. The formation of methyl nitrate is attributed to the asymmetric isomer $ONONO_2$ of N_2O_4, which is favored at high NO_2 concentration. Our *ab initio* calculations indicate that further reactions between MMH and $ONONO_2$ facilitated by the surface of the aerosol or inside can generate CH_3ONO_2, CH_3N_3 and N_2O, products observed in NO_2-rich experimental conditions. This study illustrates the heterogeneous nature of the pre-ignition reactions between MMH and NO_2.

Acknowledgments

This material is based upon work supported by, or in part by, the U. S. Army Research Laboratory and the U. S. Army Research Office under grant number W911NF-08-1-0124. The computational facility was funded by DURIP grants from ARO and ONR.

Appendix A. Supplementary material

Supplementary data associated with this article can be found, in the online version, at http://dx.doi.org/10.1016/j.combustflame.2013.01.012.

References

[1] E.W. Schmidt, in: Hydrazine and Its Derivatives: Preparation, Properties, Applications, second ed., Wiley-Interscience, New York, vol. 1, 2001.
[2] M.J. Nusca, R.S. Michaels, in: Utility of Computational Modeling for the study of Combustion Instability in Small MMH-NTO Liquid Rocket Engines, 43rd AIAA/ASME/SAE/ASEE Joint Propulsion Conference and Exhibit, Cincinnati, OH, Cincinnati, OH, 2007.
[3] M.J. Nusca, R.S. Michaels, in: Proceedings of the 50th JANNAF Propulsion Meeting, 2002, vol. 1, pp. 179–191.
[4] M.J. Nusca, in: Computational Model of Impinging-Stream/Swirl Injectors in A Hypergolic Fuel Engine, AIAA/ASME/SAE/ASEE Joint Propulsion Conference and Exhibit, Huntsville, AL, Huntsville, AL, 2003.
[5] M.J. Nusca, R.S. Michaels, in: 40th AIAA/ASME/SAE/ASEE Joint Propulsion Conference, Reston, VA, Institute of Aeronautics and Astronautics (AIAA): Reston, VA, 2004.
[6] W.A. Anderson, M.J. McQuaid, M.J. Nusca, A.J. Kotlar, A Detailed, Finite-Rate, Chemical Kinetics Mechanism for Monomethylhydrazine-Red Fuming Nitric Acid Systems; ARL-TR-5088, U.S. Army Research Laboratory, Aberdeen, MD, 2010.
[7] M.J. McQuaid, Y. Ishikawa, J. Phys. Chem. A 110 (18) (2006) 6129–6138.
[8] C.-C. Chen, M.J. Nusca, M.J. McQuaid, Modeling Combustion Chamber Dynamics of Impinging Stream Vortex Engines Fueled With Hydrazine-Alternative Hypergols; NTIS-ADA503941, U.S. Army Research Laboratory, Aberdeen Proving Ground, 2008.
[9] Y. Ishikawa, M.J. McQuaid, Theochem. -J. Mol. Struct. 818 (1–3) (2007) 119–124.
[10] J.A. Vanderhoff, W.R. Anderson, A.J. Kotlar, in: Dark Zone Modeling of Solid Propellant Flames, Proceedings of 29th JANNAF Combustion Subcommittee Meeting, Hampton, VA, Hampton, VA, 1992, pp. 225–237.
[11] G.P. Smith, D.M. Golden, M. Frenklach, N.W. Moriarty, B. Eiteneer, M. Goldenberg, C.T. Bowman, R.K. Hanson, S. Song, W.C. Gardiner, V.V. Lissianski, Z. Qin, GRI-MECH 3.0, <http://www.me.berkeley.edu/gri_mech/> (accessed February 2011).
[12] L. Catoire, T. Ludwig, X. Bassin, G. Dupr, C. Paillard, Proc. Combust. Inst. 27 (2) (1998) 2359–2365.
[13] L. Catoire, N. Chaumeix, C. Paillard, J. Propul. Power 20 (1) (2004) 87–92.
[14] M.J. McQuaid, W.R. Anderson, A.J. Kotlar, M.J. Nusca, Y. Ishikawa, in: K. Kuo, (Ed.), Proceedings of the Sixth International Symposium on Special Topics in Chemical Propulsion, 2005.
[15] S.Q. Wang, S.T. Thynell, Combust. Flame 159 (1) (2012) 438–447.
[16] T.F. Seamans, M. Vanpee, V.D. Agosta, AIAA J. 5 (9) (1967) 1616–1624.
[17] S.W. Mayer, D. Taylor, L. Schieler, Combust. Sci. Technol. 1 (2) (1969) 119–129.
[18] M.A. Saad, M.A. Sweeney, M.b. Detweile, AIAA J. 10 (8) (1972) 1073–1078.

[19] P. Breisach, H.H. Takimoto, G.C. Denault, W.A. Hicks, Combust. Flame 14 (1–3) (1970) 397–403.
[20] I.A. Leenson, J. Chem. Educ. 77 (12) (2000) 1652.
[21] Y. Zhao, D.G. Truhlar, Theor. Chem. Acc. 120 (1–3) (2008) 215–241.
[22] D.J. Tannor, B. Marten, R. Murphy, R.A. Friesner, D. Sitkoff, A. Nicholls, M. Ringnalda, W.A. Goddard, B. Honig, J. Am. Chem. Soc. 116 (26) (1994) 11875–11882.
[23] Jaguar, Schrodinger, LLC, New York, NY, 2007.
[24] M. Valiev, E.J. Bylaska, N. Govind, K. Kowalski, T.P. Straatsma, H.J.J. Van Dam, D. Wang, J. Nieplocha, E. Apra, T.L. Windus, W. de Jong, Comput. Phys. Commun. 181 (9) (2010) 1477–1489.
[25] S. Hirata, J. Phys. Chem. A 107 (46) (2003) 9887–9897.
[26] H. Blend, J. Chem. Phys. 53 (12) (1970) 4497.
[27] B. Smith, in: Infrared Spectral Interpretation: A Systematic Approach, CRC Press LLC, Boca Raton, FL, 1999, pp. 25.
[28] F.A. Miller, C.H. Wilkins, Anal. Chem. 24 (8) (1952) 1253–1294.
[29] G. Socrates, Infrared and Raman Characteristic Group Frequencies, Tables and Charts, third ed., J. Wiley & Sons, New York, 2001. pp. 195.
[30] S.K. Chung, L.B. Dunn, The Journal of Organic Chemistry 49 (5) (1984) 935–939.
[31] L.S. Rothman, D. Jacquemart, A. Barbe, D. Chris Benner, M. Birk, L.R. Brown, M.R. Carleer, J.C. Chackerian, K. Chance, L.H. Coudert, V. Dana, V.M. Devi, J.M. Flaud, R.R. Gamache, A. Goldman, J.M. Hartmann, K.W. Jucks, A.G. Maki, J.Y. Mandin, S.T. Massie, J. Orphal, A. Perrin, C.P. Rinsland, M.A.H. Smith, J. Tennyson, R.N. Tolchenov, R.A. Toth, J. Vander Auwera, P. Varanasi, G. Wagner, J. Quant. Spectrosc. Radiat. Transfer 96 (2) (2005) 139–204.
[32] R.H. Kagann, A.G. Maki, J. Quant. Spectrosc. Radiat. Transf. 30 (1) (1983) 37–44.
[33] M. Khlifi, P. Paillous, P. Bruston, F. Raulin, J.C. Guillemin, Icarus 124 (1) (1996) 318–328.
[34] J.C.D. Brand, T.M. Cawthon, J. Am. Chem. Soc. 77 (2) (1955) 319–323.
[35] F.L. Rook, J. Chem. Eng. Data 27 (1) (1982) 72–73.
[36] D.A. Stone, Toxicol. Lett. 49 (1989) 349–360.
[37] J.R. Durig, T.K. Gounev, C. Zheng, A. Choulakian, V.N. Verma, J. Phys. Chem. A 106 (14) (2002) 3395–3402.
[38] E.A. Lawton, C.M. Moran, J. Chem. Eng. Data 29 (3) (1984) 357–358.
[39] D. Luckhaus, M. Quack, J. Mol. Struct. 293 (1993) 213–216.
[40] L.H. Jones, R.M. Badger, G.E. Moore, J. Chem. Phys. 19 (12) (1951) 1599–1604.
[41] M.N. Ackermann, J.J. Burdge, N.C. Craig, J. Chem. Phys. 58 (1973) 203.
[42] W.J. Jones, N. Sheppard, Proc. R. Soc. London. Ser. A, Math. Phys. Sci. 304 (1477) (1968) 135–155.
[43] L. Catorie, N. Chaumeix, S. Pichon, C. Paillard, J. Propul. Power 22 (1) (2006) 120–126.
[44] V.G. Kravets, C. Meier, D. Konjhodzic, A. Lorke, H. Wiggers, J. Appl. Phys. 97 (2005) 084306.
[45] G. da Silva, E.M. Kennedy, B.Z. Dlugogorski, J. Phys. Chem. A 110 (39) (2006) 11371–11376.
[46] C.R. Dennis, A.J. Van Wyk, S.S. Basson, J.G. Leipoldt, Inorg. Chem. 26 (2) (1987) 270–272.
[47] F.-M. Tao, J. Chem. Phys. 108 (1998) 193–202.
[48] M. Luria, B. Cohen, Atmos. Environ. 14 (6) (1980) 665–670.
[49] J.A. Lloyd, K.J. Heaton, M.V. Johnston, J. Phys. Chem. A 113 (17) (2009) 4840–4843.
[50] S.N. Eustis, A. Whiteside, D. Wang, M. Gutowski, K.H. Bowen, J. Phys. Chem. A 114 (3) (2009) 1357–1363.
[51] W.G. Liu, S. Dasgupta, S.V. Zybin, W.A. Goddard, J. Phys. Chem. A 115 (20) (2011) 5221–5229.
[52] C.C. Addison, Chem. Rev. 80 (1) (1980) 21–39.
[53] B.J. Finlayson-Pitts, L.M. Wingen, A.L. Sumner, D. Syomin, K.A. Ramazan, Phys. Chem. Chem. Phys. 5 (2) (2003) 223–242.
[54] W.-G. Liu, W.A. Goddard, J. Am. Chem. Soc. 134 (31) (2012) 12970–12978.
[55] K.Y. Lai, R.S. Zhu, M.C. Lin, Chem. Phys. Lett. 537 (2012) 33–37.
[56] R. Svensson, E. Ljungstrom, O. Lindqvist, Atmos. Environ. 21 (7) (1987) 1529–1539.
[57] C. England, W.H. Corcoran, Ind. Eng. Chem. Res. 13 (4) (1974) 373–384.
[58] A.M. Fairlie, J.J. Carberry, J.C. Treacy, J. Am. Chem. Soc. 75 (15) (1953) 3786–3789.
[59] Nitrogen Tetroxide, Hercules Inc.: Wilmington, Del., 1968.
[60] H.W. Lucien, J. Am. Chem. Soc. 80 (17) (1958) 4458–4460.
[61] L.P. Cheng, W.Q. Cao, J. Mol. Model. 13 (10) (2007) 1073–1080.